

LASER INTERFEROMETER GRAVITATIONAL WAVE OBSERVATORY  
- LIGO -  
CALIFORNIA INSTITUTE OF TECHNOLOGY  
MASSACHUSETTS INSTITUTE OF TECHNOLOGY

Technical Note	LIGO-T1500123-v1	2015/08/04
<b>Detector Characterization of the LIGO 40m Prototype Interferometer</b>		
Eve Chase Mentors: Koji Arai and Maximiliano Isi		

**California Institute of Technology**  
**LIGO Project, MS 18-34**  
**Pasadena, CA 91125**  
Phone (626) 395-2129  
Fax (626) 304-9834  
E-mail: info@ligo.caltech.edu

**Massachusetts Institute of Technology**  
**LIGO Project, Room NW22-295**  
**Cambridge, MA 02139**  
Phone (617) 253-4824  
Fax (617) 253-7014  
E-mail: info@ligo.mit.edu

**LIGO Hanford Observatory**  
**Route 10, Mile Marker 2**  
**Richland, WA 99352**  
Phone (509) 372-8106  
Fax (509) 372-8137  
E-mail: info@ligo.caltech.edu

**LIGO Livingston Observatory**  
**19100 LIGO Lane**  
**Livingston, LA 70754**  
Phone (225) 686-3100  
Fax (225) 686-7189  
E-mail: info@ligo.caltech.edu

**Abstract**

The Advanced Laser Interferometer Gravitational-Wave Observatory (aLIGO) detectors will come online in the fall of 2015 with the goal of providing the first direct detection of gravitational waves. Detector characterization techniques, focused on the reduction of noise, are imperative to analyze and suppress noise to provide sufficient sensitivity for the detection of gravitational waves. Caltech houses the LIGO 40 meter prototype interferometer, a copy of the LIGO interferometers, providing the perfect playground to test and design novel detector characterization techniques for later implementation at the main sites. While summary pages, websites showing the state of the detector in real-time, are used to monitor the main detectors, the 40 meter prototype lacks many of these low-latency monitoring features. We incorporate new features into the 40 meter prototype summary pages in the hope of benefiting the entire LIGO community by providing real-time access to detector monitoring tools. Additionally, we develop basic tools to distinguish between gravitational wave signals and non-Gaussian noise sources, which are often misidentified as false-positive gravitational wave signals.

# Contents

<b>1</b>	<b>Introduction</b>	<b>3</b>
<b>2</b>	<b>Summary Pages</b>	<b>4</b>
2.1	Improvements to Existing Plots . . . . .	6
2.2	Additions to the Summary Pages . . . . .	7
<b>3</b>	<b>Non-Gaussianity Tests of Noise Sources</b>	<b>7</b>
3.1	Current Progress . . . . .	9
<b>4</b>	<b>Conclusion</b>	<b>12</b>
<b>5</b>	<b>Work Timeline</b>	<b>13</b>
<b>Appendix A Relevant Statistical Concepts</b>		<b>15</b>
A.1	Arithmetic Mean . . . . .	15
A.2	Variance . . . . .	15
A.3	Standard Deviation . . . . .	15
A.4	Skewness . . . . .	15
A.5	Kurtosis . . . . .	16
A.6	RMS . . . . .	16
A.7	Fourier Transform . . . . .	16
A.8	Fast Fourier Transform . . . . .	16
A.9	Parseval's Theorem . . . . .	17
<b>Appendix B How to Access the Summary Pages</b>		<b>18</b>
<b>Appendix C Laguerre Expansion</b>		<b>18</b>

# 1 Introduction

Einstein's General Theory of Relativity propelled a scientific hunt for the detection of gravitational waves. Einstein's equations establish the dynamics of space-time, a four-dimensional mathematical model combining the dimensions of space and time. General relativity predicts the existence of gravitational waves, propagating ripples in space-time. Gravitational waves are transverse waves, predicted to travel at the speed of light, produced by the change in quadrupole moment of mass distribution [1]. Nearly a century after their inception, gravitational waves have yet to be directly detected.

A worldwide network of ground-based interferometers has been constructed to provide the first direct detection of gravitational waves. The Laser Interferometer Gravitational-Wave Observatory (LIGO), consisting of detectors in Livingston, Louisiana and Hanford, Washington, recently underwent years of upgrades to provide greater sensitivity and increase the likelihood of detecting gravitational waves. A gravitational wave detector is a massive Michelson interferometer, with arm lengths of up to 4km (Figure 1) [3]. Laser light is split and sent down two orthogonal arms of equal length; the light is reflected at the end of the arms and then recombined. When a gravitational wave passes through an interferometer, a slight change in arm length will occur, resulting in a phase difference in laser light split down each arm. Gravitational wave signals are extracted from this resultant phase difference.

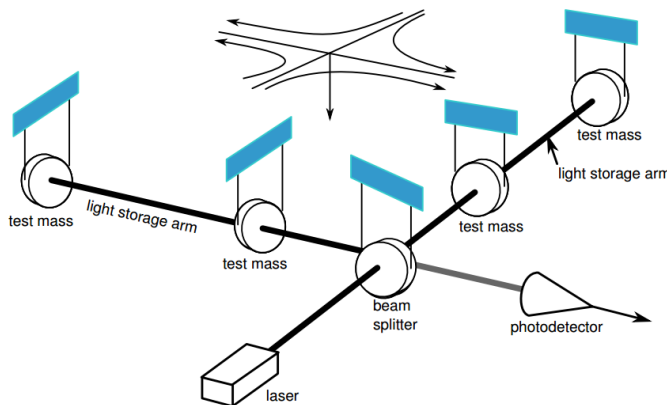


Figure 1: Basic interferometer design (LIGO [2])

Detecting a gravitational wave is difficult and requires impeccably sensitive instrumentation and detection abilities, in an attempt to detect length variations of only  $10^{-18}$  m, smaller than a proton [3]. Noise makes detection even more difficult; everything in the interferometer system is moving or fluctuating, such as the mirror position, laser frequency, laser intensity, arm resonant condition, and many more factors resulting in a substantial number of noise sources. Gravitational wave detection is a battle against noise, and detector characterization spearheads this battle. Through detector characterization, we analyze interferometer output and noise sources for certain periods of time to characterize the nature of noise, in hopes of eliminating it from the data supply. Gravitational waves cannot be detected with LIGO without strong detector characterization techniques.

As Advanced LIGO becomes operational in late 2015 [4], the implementation of advanced

detector characterization techniques is imperative to utilize the increased sensitivity for direct detection of gravitational waves. I am pleased to have devoted my summer to LIGO detector characterization while it serves a vital role in the effort to detect gravitational waves.

My summer project consists of two main parts, outlined in this paper. As described in Section 2, I am updating the LIGO summary pages which accomplish detector monitoring tasks. Subsequently, I hope to characterize non-Gaussian noise through various statistical methods, as described in Section 3. I provide a timeline for the past and future work in Section 5. Relevant statistical concepts are listed in Appendix A, and instructions for accessing and editing the summary pages are found in Appendix B.

## 2 Summary Pages

In addition to the two large LIGO detectors in Washington and Louisiana, Caltech houses a prototype detector [5]. The prototype detector, with 40m long interferometer arms, has a similar configuration to the larger detectors but is open to modification and testing of new design implementations (Figure 2). The 40m prototype detector is the perfect playground for detector characterization experimentation. By implementing new designs at the 40m detector instead of the LIGO sites, we are able to provide novel improvements to all LIGO detectors without interfering with data collection at the sites. The prototype consists of several subsystems which monitor the functionality of the detector, enumerated in Table 1 [6, 7, 8]. By frequently collecting data from the subsystems, we provide a means of monitoring the detector.

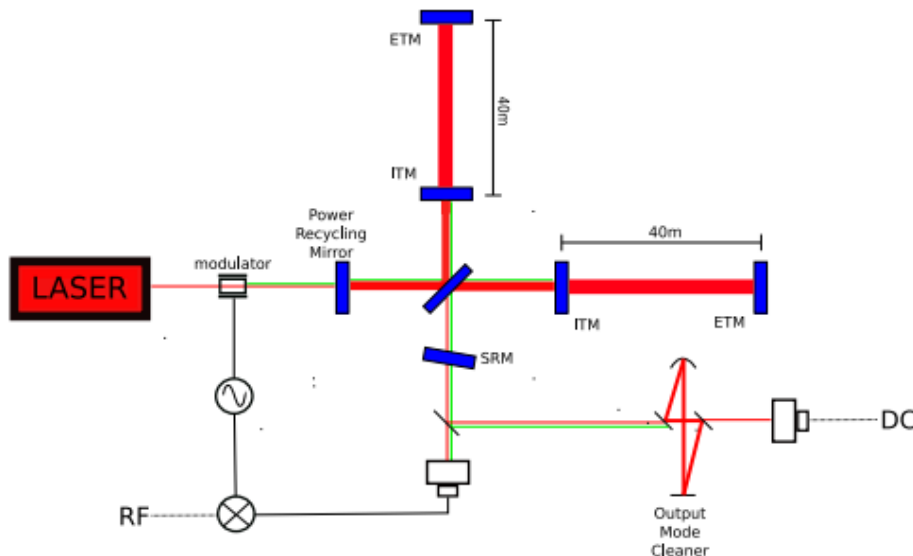


Figure 2: Schematic representation of the 40m prototype detector. A length of 40m separates the input mirror (ITM) and end mirror (ETM) [6] (Ward et al. [5]).

LIGO summary pages provide an accessible method to monitor the detectors in real time on-line [9]. Summary pages include dozens of plots monitoring detector status from seismic

Table 1: 40m Detector Subsystems

Name	Subsystem Details
Length Sensing and Control (LSC)	Mirror position control and gravitational wave signal channel.
Angular Sensing and Control (ASC)	Mirror angular control.
Arm Length Stabilization (ALS)	Monitor x and y arm length.
Pre-Stabilized Laser (PSL)	Optical cavities for laser stabilization in frequency and spacial distribution.
Input and Output Optics (IOO)	Similar to PSL.
Suspensions (SUS)	Sensors for mirror positions and angles. Optical lever system which provides additional angular sensing signals.
Physical Environmental Sensors (PEM)	Seismic and acoustic noise.
Vacuum System (VAC)	Vacuum status monitoring.

activity, to glitches, and to lock status. Summary pages include ASD spectra displaying gravitational wave amplitude spectral density over frequency [10]. Summary pages also provide time-frequency event plots representing signal-to-noise ratio (SNR) for several event triggers [10]. A screenshot of summary pages is shown in Figure 3. While the Hanford and Livingston detectors utilize summary pages, the 40m detector has few features implemented on the summary pages and many of the already-existing plots are flawed. The 40m summary pages are far behind the quality of the Livingston and Hanford summary pages and lack much of the information represented in the latter two [9, 11, 12]. We hope to provide a legible, informative summary page interface to improve upon the currently existing channel visualization for the 40m prototype.

Implementation of summary pages for the 40m prototype requires careful configuration of many channels from many subsystems of the prototype. We analyze each channel for a set period of time to determine the nature of each signal. While checking the behavior of signals, we may reveal problems with the functionality of specific subsystem of the detector, contributing to detector improvement.

Summary pages are produced using the GWsumm toolbox, which is based on the GWpy Python package which provides tools to load, assess, and plot LIGO data. GWsumm scripts can provide plots for data channels and associated HTML to post the plots on the summary page website. A significant portion of my summer is devoted to characterizing data channels for the 40m detector and implementing them into the summary page system.

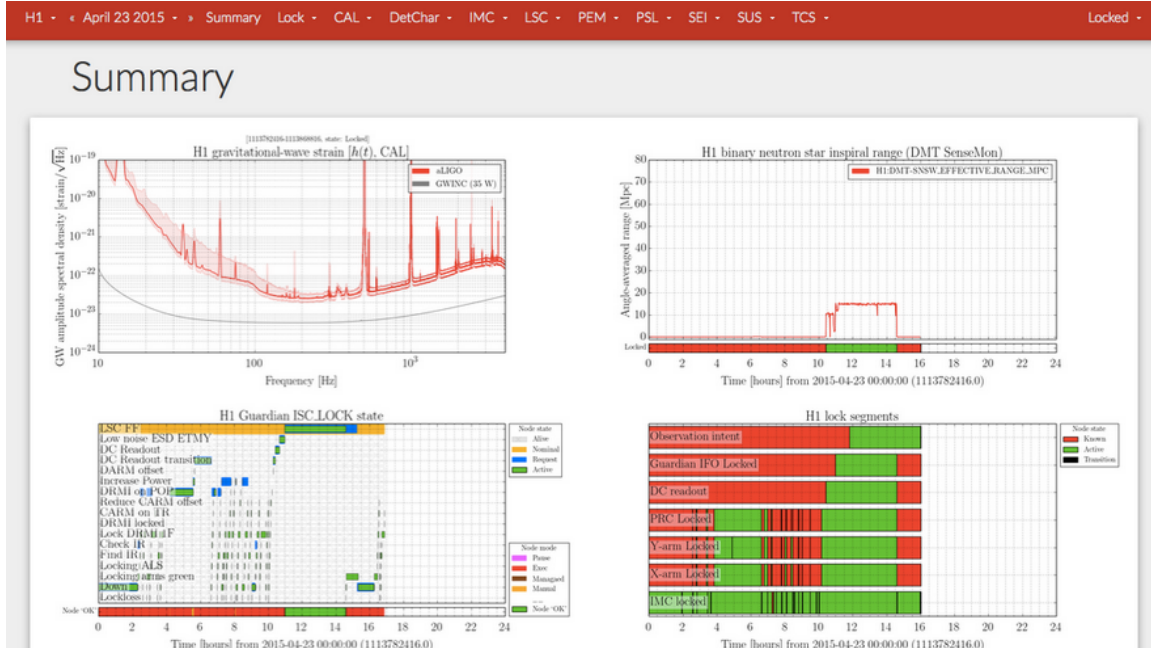


Figure 3: Screenshot of a summary page monitoring the Hanford detector [12].

## 2.1 Improvements to Existing Plots

While the 40m detector summary pages provide a basic foundation to reach the level of effective data display and quality of information as the Livingston and Hanford summary pages, many necessary features have yet to be implemented. Several plots are already available on the summary pages, including those for IOO, PEM, PSL, SUS, and VAC subsystems, but many of these plots require improvements. As many plots lacked titles and axis labels, I began my summer work with a simple introduction to the code behind the summary pages with the addition of improved titles and axis labels. Through this work, I was able to gain familiarity with the code and ensure that my changes appeared on the summary pages website in real time.

In addition to providing cosmetic adjustments to either the dearth or flaws in labels, I altered the range of axes in many cases. Occasionally, axis ranges that fail to appropriately display the necessary data are selected. I determined appropriate axis ranges by observing past data from several months at a time on the DataViewer program present at the 40m detector, and I implemented appropriate axis ranges into the summary pages.

There are several periods of time during which no data is displayed on the summary pages, causing confusion as to what is causing the break in data and uncertainty if data is not being collected or if the data collected is not within the axis ranges of the summary page plots. By monitoring the channels in question on DataViewer, I can analyze the cause of such breaks in data acquisition and implement changes to the summary pages, appropriately.

We believe that the summary pages lack accurate triggering systems for certain plot rendering processes. The value of certain channels determine if other channels should be plotted in the summary pages. For example, for channels C1:LSC-XARM\_OUT\_DQ and

C1:LSC-YARM\_OUT\_DQ to be plotted in the Arm LSC Control signals figures, C1:LSC-TRX\_OUT\_DQ and C1:LSC-TRY\_OUT\_DQ must be higher than 0.5, thus acting as triggers. I will implement several necessary triggers to the summary pages, if not already implemented. Furthermore, for all existing triggers, I will provide a graphical indicator informing viewers that data is not being represented at a certain time for specific plots.

## 2.2 Additions to the Summary Pages

We hope to provide useful and informative additions to the summary pages to help all users of the 40m detector. I will speak with many of the frequent users of the 40m detector and implement improvements to the summary pages that they view as necessary. This ensures that we provide useful information on the summary pages.

As some interest was expressed in improving plots for suspension systems, I added plots to these sections of the summary pages. Six suspension system optical level (OpLev) plots already exist on the summary pages and represent optical lever fluctuations in microradians over time for numerous channels. I produced spectra for each OpLev plot and displayed the spectra tangentially to the already existing timeseries, to provide an easy means of visually comparing the data.

In addition to these enumerated improvements, I am open to the possibility of more creative projects using the summary page interface. I could introduce interactive plots allowing for such features as zooming in or scrolling through different axis ranges of the data. Furthermore, I could introduce new types of plots, such as a coherogram to better display information.

## 3 Non-Gaussianity Tests of Noise Sources

While not working on implementation of summary pages, I focus on noise characterization. We explore the appearance of various noise sources in the interferometer channels and provide additional methods to characterize noise with the predefined goal of eliminating as many noise sources as possible from the detector.

Gravitational wave detectors are constantly inundated with noise. Noise comes in numerous forms, such as white noise, sinusoidal, stochastic, Gaussian, and more. Sources of white noise include quantum noise and electronic noise with broad frequency bands. Sinusoidal noise sources such as narrow band sources and noise from power lines at 60Hz are also present, in addition to narrow band stochastic noise sources such as thermal noise in mirror suspension wires. Other sources of noise include seismic noise. We can categorize noise as Gaussian or non-Gaussian, dependent on the statistical nature of the noise. Typically, thermal and quantum noise exhibit Gaussian behavior. It is difficult to distinguish between gravitational wave events and non-Gaussian noise, specifically in gravitational wave searches without predefined waveforms (i.e. burst searches), thus requiring the characterization of non-Gaussian noise to reveal true event signals [13]. By characterizing noise Gaussianity, we can better recognize noise patterns and understand the nature of noise, leading to the further elimination of many noise sources.



Power spectral density (PSD) provides one means to characterize noise distributions. A PSD is a measure of power in several frequency bands, averaged over time. Following a Fourier transform of a timeseries  $x(t)$  we receive the following function in the frequency-domain:

$$\tilde{x}(f) = \int_{-\infty}^{\infty} x(t)e^{-i2\pi ft} dt, \quad (1)$$

where  $|\tilde{x}(f)|^2$  provides the energy spectral density. Energy spectral density follows Parseval's theorem, described in Appendix A. When noise extends infinitely in the time domain, we can define the PSD [16, 17, 18]:

$$\lim_{T \rightarrow \infty} \frac{1}{T} |\tilde{x}_T(f)|^2. \quad (2)$$

PSDs also follow Parseval's theorem and correct calculation of a PSD can be confirmed using this theorem. A PSD has units equivalent to the units of  $|x(t)|^2$  divided by Hz. Typically, in gravitational wave data analysis, we represent our PSDs in strain /  $\sqrt{\text{Hz}}$ . This requires us to take the square root of our PSD, which forms an amplitude spectral density (ASD). Colloquially, ASDs are often still called PSDs, despite this change in calculation.

We calculate PSDs of interferometer signals for a given short period of time, providing many useful applications in detector characterization. For example, PSD calculation allows us to monitor the violin, roll, and bounce modes of the steel wires used to suspend the interferometer's mirrors. Each mirror has six rigid body degrees of freedom: longitudinal, side, vertical, pitch, yaw, and roll. The resonances of each of these six modes has low dissipation, corresponding to a long ringdown mode, or high quality factor ( $Q$ ) for the modes. Feedback damping is used to lower the  $Q$ 's for some modes, but the violin, roll, and vertical (or bounce) modes have no such damping control and occasionally become excited by seismic motion or cross-coupling between modes. Characterization of noise from these three modes can be achieved through the calculation of a PSD.

By following the statistical method, enumerated in Ando et al. [13], we statistically characterize Gaussianity of PSDs. Assuming we sample the detector output,  $v(t)$ , in time intervals of  $\Delta t$ , the raw output data is recorded as  $v_j = v(j\Delta t)$ . From the output data, we calculate the output power:

$$P_j = |v_j|^2. \quad (3)$$

By dividing the output data into  $n$  segments, with  $k$  data points in each segment, we define the following quantities derived from power:

$$P_0 \cong \overline{P_j} \quad (4)$$

$$P_1 = \frac{1}{k} \sum_{j=1}^k P_j \quad (5)$$

$$P_2 = \frac{1}{k} \sum_{j=1}^k (P_j)^2, \quad (6)$$

where  $P_0$  is the long-term average of  $P_j$ , using all data points.  $P_1$  is the first-order moment (mean) of signal power,  $P_j$ , given for only a single data segment. Similarly,  $P_2$  is the second-order moment (variance) of  $P_j$ , also for only a specific segment. The parameter  $\overline{P_j}$ , is the

average of  $P_j$ . If data is completely stationary,  $P_j$  is constant, resulting in a  $P_1$  equal to  $P_0$  and  $P_2$  equal to  $P_0^2$  for all  $n$  data segments. From these parameters, we define two Gaussianity evaluations coefficients:

$$c_1 = \frac{P_1}{P_0} - 1 \quad (7)$$

and

$$c_2 = \frac{1}{2} \left( \frac{P_2}{P_1^2} - 2 \right), \quad (8)$$

which are also the first two coefficients in the Laguerre expansion of the noise power distribution (see Appendix C). It is assumed that  $c_2$  becomes constant if the signal power is much larger than the background noise level [13]. The coefficient  $c_1$  provides a metric for the stability of a signal, while  $c_2$  indicates non-Gaussianity, as  $\frac{P_2}{P_1^2}$  is related to glitchiness of power. Using the coefficients  $c_1$  and  $c_2$ , we can evaluate the Gaussianity of a PSD.

Rayleigh statistics provide another means to determine the Gaussianity of a noise distribution [7, 14]. The Rayleigh statistic ( $R$ ) provides a metric for the Gaussianity of noise through a calculation of the ratio of standard deviation to mean of a power spectrum in a set frequency bin:

$$R(f) = \frac{\sigma[|\tilde{x}_T(f)|^2]}{\mu[|\tilde{x}_T(f)|^2]}, \quad (9)$$

where  $\sigma$  and  $\mu$  are defined in Appendix A and  $\tilde{x}_T(f)$  is defined in Equation 1. The value of  $R$  provides a numerical measure of the Gaussianity of a signal, with  $R = 1$  representing Gaussian noise,  $R < 1$  representing coherent variation in the data, and  $R > 1$  indicating that glitchy data is present [7, 14]. The RayleighMonitor algorithm can be used to plot spectrograms ( $\mu$ ) and Rayleighgrams ( $R$ ) for a visual representation of detector characterization [14, 15].

We calculate both Rayleigh statistics and PSDs for interferometer signals at each predetermined frequency segment and plot PSD and  $R$  in the same figure. We are interested in determining the relationship between Rayleigh statistics and PSDs, with a specific focus on the Gaussianity method outlined in Ando et al. [13]. By characterizing the Gaussianity of noise, we hope to provide a better understanding of noise sources at the interferometer and eliminate these noise sources in data requisition.

### 3.1 Current Progress

I have begun calculating PSDs from previous LIGO data using a Python program. I downloaded an hour of Livingston S5 data from the LIGO Open Science Center as an hdf5 file. Using the readligo module, also available at the LIGO Open Science Center, I stored this data into a series of Python data structures. The data files include information on strain, time, and channel information.

By plotting strain versus time, I produced a timeseries for 16 seconds of data this hour-long period (Figure 4). The data is chaotic and conveys little information in the time-domain.

Some oscillatory periods can be determined from this plots, but much more information is available if we observe the same dataset in the frequency-domain.

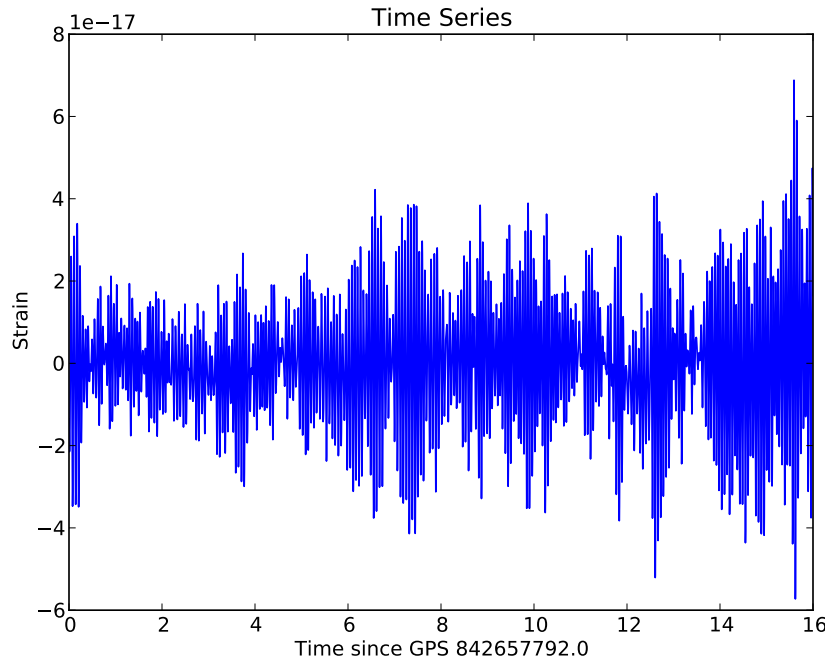


Figure 4: Strain versus time for 16 seconds of L1 data from S5.

We create a PSD of the dataset to provide more information about the frequency content of the timeseries. We use the Python function, `matplotlib.mlab.psd()` to compute the PSD. This function uses Welch’s average periodogram method to approximate a PSD. The time-series is divided into several segments of length  $NFFT$ , and the fast Fourier transform (see Appendix A) is calculated for each segment, then squared, and then averaged for all segments to produce the PSD. We define the sampling frequency to be the inverse of the time between consecutive data sampling. The  $NFFT$  segment length is also set to this sampling frequency value. We select a Hanning window function, which maps each segment’s values onto the Hanning function of length  $NFFT$ . As the Hanning function eliminates datapoints at the endpoints of segments, we define an overlap of half of  $NFFT$  which recalculates the PSD using the same segments shifted over by half their lengths. Using this method, we produce the PSD seen in Figure 5. This produced PSD looks very similar to that of the Livingston detector during the S5 run, with several frequency peaks appearing in the expected locations (Figure 6). To directly compare Figure 5 and Figure 6, the y-axis of Figure 6 must be divided by the length of the interferometer arms, 4km. We confirm the calculation of our PSD by ensuring that Parseval’s theorem holds, by following Equation 23 in Appendix A.

We begin to explore the Gaussianity of LIGO data at individual time values by compiling distribution statistics for a series of PSDs. We split the timeseries of Figure 4 into several equally spaced frequency segments and calculate the individual PSD of each chunk, altering the  $NFFT$  length accordingly. We plot the PSD produced for each segment on the same plot and compare them (Figure 7). We provide a more quantitative metric of comparison by

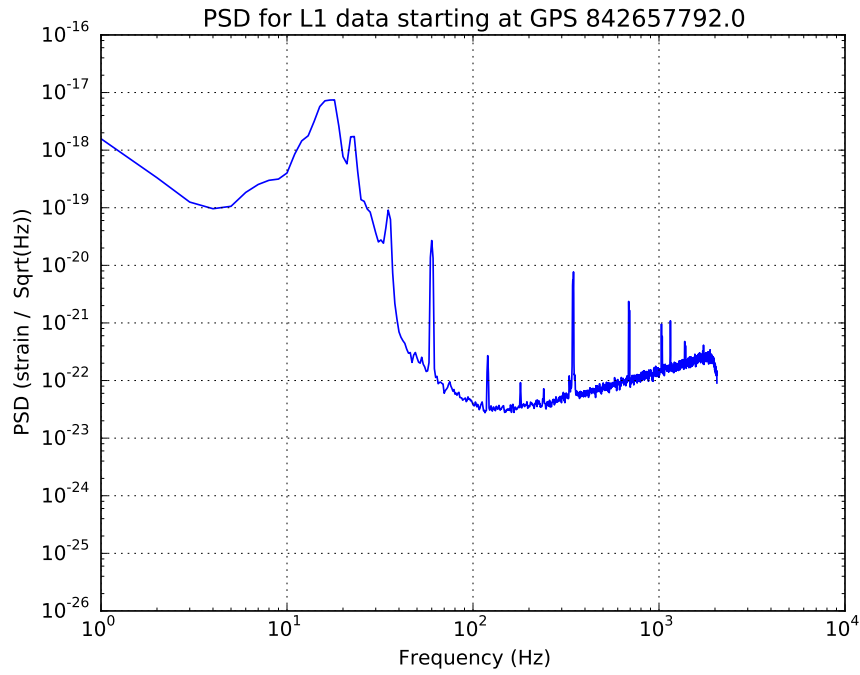


Figure 5: PSD calculated over entire timeseries dataset.

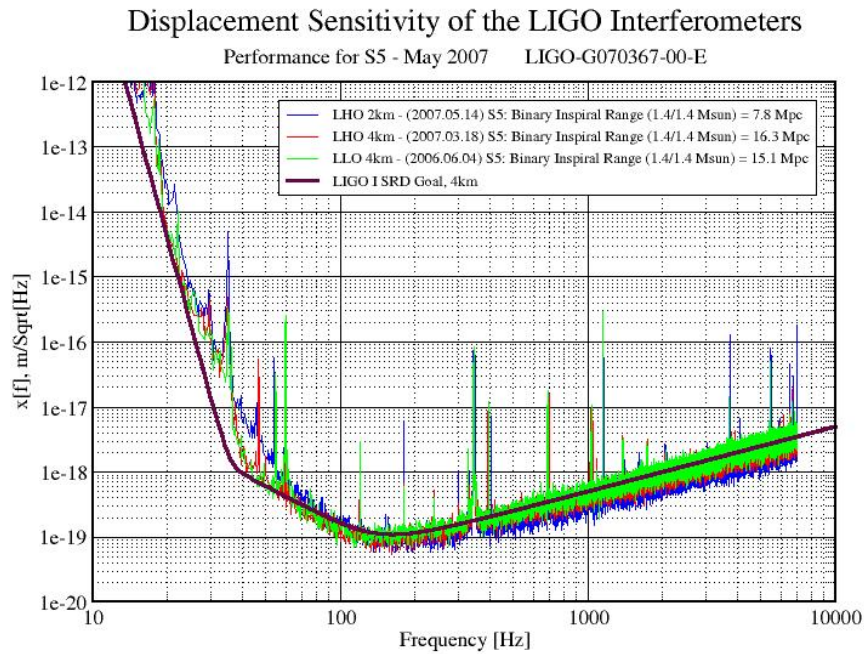


Figure 6: Published sensitivity for the LIGO detectors during the S5 run (LIGO [19]).

calculating the mean and standard deviation of the spread in PSD values at one particular frequency,  $f_0$ . By calculating the mean at each frequency bin, we reproduce the original PSD. In Figure 8, we plot the mean and standard deviation spread for each frequency bin. We will continue analysis with this data set by following the methods outlined in Ando et al. [13] to provide a statistical representation of Gaussianity in the PSD.

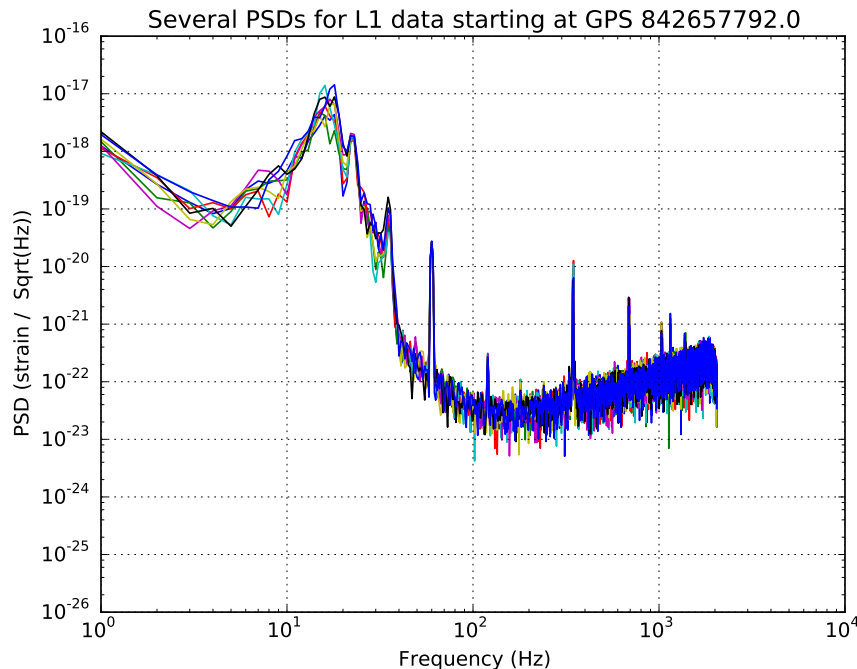


Figure 7: Several PSDs calculated for equally spaced frequency segments and compiled into one graph.

## 4 Conclusion

As Advanced LIGO begins to collect data, detector characterization takes a vital role in the effort to locate gravitational wave signals in this data. It is imperative to distinguish between gravitational wave events and non-Gaussian noise signals in order to detect gravitational waves, specifically bursts [13]. The implementation of summary pages for the 40m prototype detector benefits the entire LIGO community by providing real-time access to detector monitoring tools for the interferometer and providing improvements to the summary pages, which may be incorporated into summary pages for the main detectors. In the upcoming race to directly detect gravitational waves with a ground-based interferometer, detector characterization is vital in the understanding and elimination of noise.

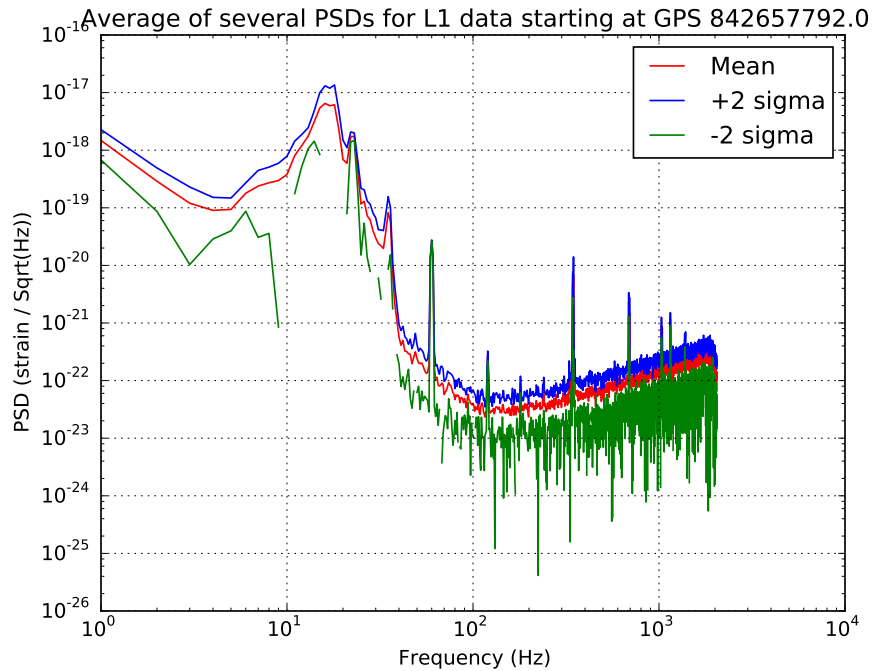


Figure 8: The mean and standard deviation bands for all PSDs in Figure 7 each frequency bin.

## 5 Work Timeline

A timeline for my summer work can be found in Table 2.

## References

- [1] Flanagan, E. & S. Hughes. *The basics of gravitational wave theory*. New J.Phys. 7, 204 (2005).
- [2] [http://www.ligo.caltech.edu/LIGO\\_web/PR/scripts/draw\\_lg.html](http://www.ligo.caltech.edu/LIGO_web/PR/scripts/draw_lg.html)
- [3] Abbott, BP et al. *LIGO: the Laser Interferometer Gravitational-Wave Observatory*. Rep. Prog. Phys. 72, 076901 (2009).
- [4] <https://www.advancedligo.mit.edu/>
- [5] Ward, RL et al. *DC Readout Experiment at the Caltech 40m Prototype Interferometer*. Class. Quantum Grav. 25, 114030 (2008).
- [6] Izumi, K. et al. *Multicolor cavity metrology*. J. Opt. Soc. Am. 29, 10, 2092 (2012).
- [7] Davison, E. *Detector Characterization Tools for Interferometer Commissioners*. LIGO SURF 2012.

Table 2: Agenda for work throughout the summer

Week	Task
Week 1	Review signal processing techniques; Tour 40m detector; View several channels on DataViewer
Week 2	Calculate PSDs; Intro to summary pages
Week 3	Minor changes to summary pages; Calculate OpLev channel spectra
Week 4	Add plots to summary pages; Calculate statistics for PSDs
Week 5	Create personal summary pages; Add CDS tab to personal summary pages
Week 6	Tour LLO; Investigate duty plots and states; Theoretical investigation of Gaussianity
Week 7	Add LSC, ASC, and ALS tabs to summary pages; Addition of states to summary pages; Theoretical investigation of Gaussianity
Week 8	Addition of new plots to summary pages; Addition of states to summary pages; Gaussianity investigations with PSDs
Week 9	Addition of new plots to summary pages; Gaussianity investigations with PSDs; Calculation of Rayleigh statistics
Week 10	Gaussianity investigations with PSDs; Calculation of Rayleigh statistics; Final presentation

[8] Abbott, B. et al. *LIGO Caltech 40-Meter Prototype Procedures Manual*. 2003.

[9] <http://www.ligo.caltech.edu/~misi/summary/>

[10] Macleod. *How to read the (LIGO) summary pages*.

[11] <https://ldas-jobs.ligo-la.caltech.edu/~detchar/summary/>

[12] <https://ldas-jobs.ligo-wa.caltech.edu/~detchar/summary/>

[13] Ando, M. et al. *Methods to characterize non-Gaussian noise in TAMA*. *Class. Quantum Grav.* 20, S697 (2003).

[14] Sutton, P. & P. Saulson. *RayleighMonitor Overview*. LIGO-G040422-00-Z.

[15] Finn, L., Gonzalez, G. & P. Sutton. *RayleighMonitor: A Time-Frequency Gaussianity Monitor for the DMT*. LIGO-G020133-00-Z (2002).

- [16] Kanner, J. *Introduction to LIGO data analysis*. LIGO-G1500862 (2015).
- [17] Shawhan, P. *Gravitational-Wave Data Analysis: Lecture 1*. (2012).
- [18] Blandford, R. & K. Thorne. Random Processes. In *Applications of Classical Physics*. (2012).
- [19] [http://www.ligo.caltech.edu/~ll\\_news/s5\\_news/s5002.jpg](http://www.ligo.caltech.edu/~ll_news/s5_news/s5002.jpg)
- [20] <http://hyperphysics.phy-astr.gsu.edu/hbase/math/fft.html>

## Appendix A Relevant Statistical Concepts

### A.1 Arithmetic Mean

The arithmetic mean represents an unweighted average of a set of  $n$  values.

$$\mu = \bar{x} = \frac{1}{n} \sum_{i=1}^n x_i \quad (10)$$

### A.2 Variance

Variance,  $\sigma^2$ , measures the spread of a set of numbers.

$$\sigma^2 = \frac{1}{n} \sum_{i=1}^n (x_i - \mu)^2 \quad (11)$$

### A.3 Standard Deviation

Standard deviation is the square root of variance. It represents the amount of variation in a set of  $n$  values.

$$\sigma = \sqrt{\frac{1}{n} \sum_{i=1}^n (x_i - \mu)^2} \quad (12)$$

### A.4 Skewness

Skewness quantifies the asymmetry of a distribution. If the left side is more pronounced than the right side, then the data set is said to have negative skewness. If the distribution is symmetric, skewness is zero. Equations for skewness vary, and one such equation is provided below.



$$Skewness = \frac{\frac{1}{n} \sum_{i=1}^n (x_i - \mu)^3}{\sigma^3} \quad (13)$$

## A.5 Kurtosis

In addition to skewness, kurtosis provides another descriptor for the shape of a distribution. Kurtosis is represented in many ways, of which one such equation is provided, and can be thought of as “peakedness” of a distribution.

$$Kurtosis = \frac{\frac{1}{n} \sum_{i=1}^n (x_i - \mu)^4}{\sigma^4} \quad (14)$$

## A.6 RMS

The root mean square (RMS) can be calculated to represent a series of data points varying with time. The RMS for a set of  $n$  discrete values is:

$$x_{rms} = \sqrt{\frac{1}{n}(x_1^2 + x_2^2 + \cdots + x_n^2)}, \quad (15)$$

while the RMS for a continuous time-dependent function from the time interval  $T_1$  to  $T_2$  is

$$f_{rms} = \sqrt{\frac{1}{T_2 - T_1} \int_{T_1}^{T_2} [f(t)]^2 dt}. \quad (16)$$

## A.7 Fourier Transform

The Fourier transform provides a continuous Fourier series from  $-\infty$  to  $\infty$  for a given function. The Fourier transform of  $f(t)$  is,

$$g(\omega) = \frac{1}{2\pi} \int_{-\infty}^{\infty} f(t)e^{-i\omega t} dt, \quad (17)$$

and the inverse Fourier transform is,

$$f(t) = \int_{-\infty}^{\infty} g(\omega)e^{i\omega t} d\omega. \quad (18)$$

## A.8 Fast Fourier Transform

The fast Fourier transform (FFT) provides a computer algorithm for calculating a Fourier transform. Rather than describing the mathematical formalism of a FFT, I will express its overall function pictorially in Figure 9.

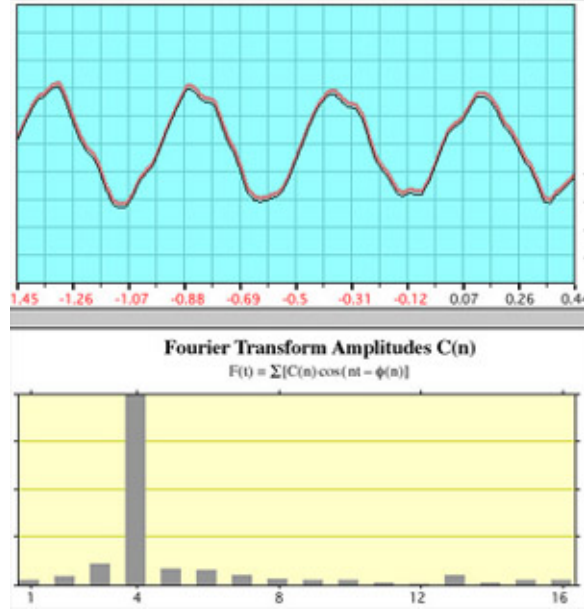


Figure 9: The bottom plot displays the FFT of the above plot. The FFT shows that most of the power is at frequency 4, reflecting the fact that four periods were chosen for the calculation of the FFT [20].

## A.9 Parseval's Theorem

Parseval's theorem illuminates the relationship between the average of the square of a function  $f(t)$  and the Fourier coefficients. Assume a function  $f(t)$  is represented by the following Fourier series:

$$f(t) = \sum_{-\infty}^{\infty} c_n e^{in\pi t/l}, \quad (19)$$

where  $c_n$  is

$$c_n = \frac{1}{2l} \int_{-l}^l f(t) e^{-in\pi t/l} dt. \quad (20)$$

Parseval's theorem then claims the following:

$$\text{The average of } |f(t)|^2 \text{ over a period} = \sum_{-\infty}^{\infty} |c_n|^2. \quad (21)$$

Parseval's theorem can be written in several different ways including the following:

$$\int_{-\infty}^{\infty} |x(t)|^2 dt = \int_{-\infty}^{\infty} |\tilde{x}(f)|^2 df, \quad (22)$$

$$\int_0^{\infty} S_y(f) df = \sigma_y^2 \quad (23)$$

where  $|\tilde{x}(f)|^2$  is the energy spectral density and  $S_y(f)$  is the power spectral density. Parseval's theorem can easily be related to the RMS by the inclusion of a square root.

## Appendix B How to Access the Summary Pages

The 40m detector summary pages can be viewed on <https://ldas-jobs.ligo.caltech.edu/~max.isi/summary/>, which updates every 30 minutes to represent the most recent channel outputs for the detector.

After receiving appropriate credentials, files to edit the summary pages can be found on [nodus.ligo.caltech.edu](http://nodus.ligo.caltech.edu) at `/users/public_html/gwsumm-config`. All files following the pattern `c1*.ini` are read by a Cron job which then applies the changes found in these files to the summary page website. These files contain information on the channels that are represented and the plot format that will represent the relevant information, such as spectra, timeseries, etc.

## Appendix C Laguerre Expansion

I provide a statistical background for Laguerre exponential expansions, following the method defined in Ando et al. [13]. We define a probability density function,  $P(\zeta)$ , given the following Rayleigh distribution:

$$\Phi(\zeta) = e^{-\zeta}, \quad (24)$$

where  $\zeta$  is a function of Gaussian variables  $x$  and  $y$ ,

$$\zeta = \frac{1}{2}(x^2 + y^2), \quad (25)$$

related to the instantaneous power  $P_j$  normalized by  $P_0$  (see Section 3). Given that  $P(\zeta)$  is perturbed from an exponential distribution, we represent the probability density function as a series expansion:

$$P(\zeta) = \bar{c}_0\Phi(\zeta) + \bar{c}_1L_1(\zeta)\Phi(\zeta) + \bar{c}_2L_2(\zeta)\Phi(\zeta) + \dots \quad (26)$$

$L_n(\zeta)$  describes the Laguerre polynomials for  $\zeta$ , following the pattern

$$L_n(\zeta) = e^\zeta \frac{d^n}{d\zeta^n} (\zeta^n e^{-\zeta}). \quad (27)$$

The first few Laguerre polynomials are explicitly described as  $L_0 = 1$ ,  $L_1 = 1 - x$ , and  $L_2 = \frac{1}{2}(x^2 - 4x + 2)$ . Laguerre polynomials satisfy a condition for orthogonality:

$$\int_0^\infty L_m(\zeta)L_n(\zeta)\Phi(\zeta)d\zeta = \delta_{mn}. \quad (28)$$

The coefficients  $\bar{c}_n$  can be calculated with

$$\bar{c}_n = \int_{-\infty}^\infty L_n(\zeta)P(\zeta)d\zeta, \quad (29)$$

resulting in coefficients such as  $\bar{c}_0 = 1$ ,  $\bar{c}_1 = 1 - \bar{\zeta}$ , and  $\bar{c}_2 = \frac{1}{2}(\bar{\zeta}^2 - 2)$ .